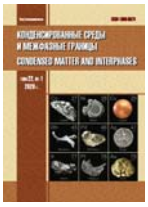

Condensed Matter and Interphases
(Kondensirovannye sredy i mezhfaznye granitsy)

Original articles

DOI: https://doi.org/10.17308/kcmf.2020.22/2528 eISSN 2687-0711
Received 29 November 2019
Accepted 15 December 2019
Published online 25 March 2020

Parameters of Oxide Films Anodically Formed on Ag-Zn Alloys with Different Concentrations of Vacancy Defects in the Surface Layer

© 2020 S. N. Grushevskaya✉, A. V. Vvedenskii, V. O. Zaitseva

Voronezh State University, 1 Universitetskaya pl., Voronezh 394018, Russian Federation

Abstract

The nature and the properties of oxide films anodically formed on metals and alloys depend on the chemical composition and energetic state of the electrode surface.

This study was aimed at revealing the composition and the parameters of oxide films formed in 0.1 M KOH on silver-zinc alloys (up to 30 at.% of Zn) with different concentrations of vacancy defects in the surface layer.

The enhanced concentration of vacancy defects in the alloys surface layer was created by preliminary selective dissolution of zinc at different potentials in 0.01 M HNO_3 + 0.09 M KNO_3. These alloys were moved into 0.1 M KOH for the formation of oxide films. The composition of films was monitored by cathodic voltammetry. The film thickness was calculated from the anodic coulometry taking into account the current efficiency. The latter was determined by cathodic coulometry. The morphology of the electrode surface was monitored by scanning electron microscopy (SEM).

It was revealed that the concentration of superequilibrium vacancies formed in the surface layer depended on the potential of the selective dissolution of zinc from the alloy. The peak of Ag(I) oxide reduction was registered on the cathodic voltammograms of the alloys after their anodic oxidation. The current efficiency of oxide formation on Ag-Zn alloys was less than 100%. It decreased with zinc concentration in the alloys. The thickness of Ag(I) oxide on alloys did not exceed 25 nm. SEM images showed the uniform distribution of oxide particles along the electrode surface. The shape of the particles was close to spherical.

The Ag(I) oxide was the main product of oxidation of silver-zinc alloys (up to 30 at% of Zn) with different vacancy defects of the surface layer. The current efficiency and the thickness of Ag(I) oxide films formed on alloys with an increased concentration of vacancy defects were less as compared with the current efficiency and the thickness of Ag(I) oxide films formed on pure silver. However, these parameters were higher as compared with the parameters of Ag(I) oxide films formed on alloys with an equilibrium concentration of vacancy defects. It was found that the diameter of the Ag(I) oxide particles decreased, and their quantity on the unit of the electrode surface increased with an increase of the concentration of vacancy defects in the alloys surface layer.

Keywords: silver-zinc alloys, Ag(I) oxide, selective dissolution, anodic oxide formation.

For citation: Grushevskaya S. N., Vvedenskii A. V., Zaitseva V. O. Parameters of oxide films anodically formed on Ag-Zn alloys with different concentrations of vacancy defects in the surface layer. *Kondensirovannye sredy i mezhfaznye granitsy = Condensed Matter and Interphases*. 20120;22(1): 48–57. DOI: https://doi.org/10.17308/kcmf.2020.22/2528

1. Introduction

Silver and zinc oxides, in particular nanosized ones, are considered to be functional materials with the desired properties [1–4]. Structures of the oxide/oxide [5, 6] or oxide/metal type [7–10] play a decisive role in anode and corrosion processes. They are also used in modern semiconductor technologies and in the manufacture of sensors. The scope of application for oxide structures is determined by a set of their main parameters, depending on the method and conditions of their preparation.

One of the possible ways to obtain the oxide phase and control its parameters is the

✉ Svetlana N. Grushevskaya, e-mail: sg@chem.vsu.ru

anodic oxidation of homogeneous alloys with different contents of their components. During the transition from individual metals to alloys, the composition of oxidation products and the structure of the oxide film become more complicated [11–13]. In addition, a number of side electrochemical reactions can occur at the potentials of oxide growth; therefore, data on the current efficiency of the anodic oxide formation process are required for the correct evaluation of its thickness. Finally, during the anodic oxidation of alloys, the possibility of their selective dissolution (SD) should be taken into account, as a result of which the electronegative component predominantly passes into the solution, and the surface zone of the alloy is enriched with the electropositive component and superequilibrium vacancies [14–17]. Due to a significant increase in the concentration of vacancies in comparison with the equilibrium concentration, the energy saturation of the system as a whole also increases, which can be reflected both in the kinetics of further oxide formation and in the properties of anodically formed oxides. The concentration of vacancy defects in the surface layer of the alloy can be controlled by changing the conditions of the SD.

The goal of this study was the calculation of the current efficiency of the anodic oxide formation and determination of the composition and thickness of oxide films anodically formed in 0.1 M KOH on silver-zinc alloys with different concentrations of vacancy defects in the surface layer.

2. Experimental

Homogeneous polycrystalline alloys were made of silver and zinc (metal purity of 99.99 at%) in vacuum quartz ampoules with exposure at a temperature of 1273 K for at least two hours and their subsequent slow cooling. Predicted zinc concentration N_{Zn} was from 5 to 30 at% (Table 1). The phase (a-phase) and chemical compositions of the alloys were confirmed by X-ray diffractometry and energy-dispersive microanalysis [18]. Samples were mounted in epoxy resin in such a way that the working surface with the geometric area S_g from 0.4 to 0.5 cm^2 remained open (Table 1). The preparation of the surface of the electrodes for the experiment included mechanical processing on abrasive paper, polishing on suede and degreasing with isopropyl alcohol.

Electrochemical studies were carried out using an IPC-Compact potentiostat (Institute of Physical chemistry and Electrochemistry, RAS, Moscow). Anodic oxide formation and determination of current efficiency were performed in 0.1 M KOH (pH 12.89), prepared on double distilled water from a chemically pure reagent and deaerated by sparging with chemically pure argon. The sequence of stages was as follows:

1. Cathodic polarization in an alkaline solution for 300 s at a potential E_c = –1.1 V for reduction of oxide traces and standardization of the surface.

2. Potential-controlled and charge-controlled anodic synthesis of Ag(I) oxide of a specified thickness (34 nm under the assumption of 100% current efficiency of the anodic formation of Ag_2O) at potential E_a = 0.56 V. This value was chosen based on the results of anodic voltammetry and corresponds to the maximum growth rate of Ag(I) oxide on silver in 0.1 M KOH [18].

3. Change of alkaline solution in a cell in a sealed argon atmosphere for the removal of soluble oxidation products of silver or zinc.

4. Potentiodynamic cathodic polarization at a scan rate of 1 mV s^{-1} from open-circuit potential E_0 to E_c.

In a separate series of experiments, after the completion of stage 2, the dependence of the open-circuit potential E_0 from time was recorded for 20 min, after the solution was changed (stage 3) and the cathodic potentiodynamic reduction of the oxidation products remaining on the electrode surface was performed (stage 4).

For the determination of the role of super-equilibrium vacancies before anodic oxide

Table 1. Symbols and the geometric surface of Ag-Zn alloys (α-phase) with different concentration of zinc N_{Zn}

N_{Zn}, at%	5	10	15	20	30
Symbol	Ag5Zn	Ag10Zn	Ag15Zn	Ag20Zn	Ag30Zn
Surface, cm^2	0.40	0.44	0.43	0.42	0.48

formation, the potential-controlled and charge-controlled SD of Ag15Zn and Ag30Zn alloys in 0.01 M HNO_3 + 0.09 M KNO_3 (pH 2.16) solution, prepared on double distilled water from chemically pure reagents and deaerated by sparging with chemically pure argon was performed. The sequence of stages was as follows:

1′. Immersion of the working electrode for 240 s in acid solution under protection potential E_c = –1.1 V, eliminating the ionization of both components for the reduction of traces of oxides and standardization of the surface.

2′. Anodic selective dissolution for 60 s at potentials E_1^{SD} = 0.4 V, E_2^{SD} = 0.5 V or E_3^{SD} = 0.6 V. Potential values were selected based on the results of anodic voltammetry (Fig. 1) and correspond to the thermodynamic stability region of the electropositive component of the alloy.

On the alloys obtained as a result of stages 1′ and 2′, the oxide was formed with the subsequent determination of the current efficiency (stages 1–4).

The current efficiency Ψ of the anodic oxidation process in all experiments was calculated as the ratio of the cathodic charge of film reduction Q_c to the anodic charge of its formation Q_a:

$$\Psi = Q_c/Q_a. \quad (1)$$

The determined current efficiency was used for the calculation of the thickness of the formed oxide layer:

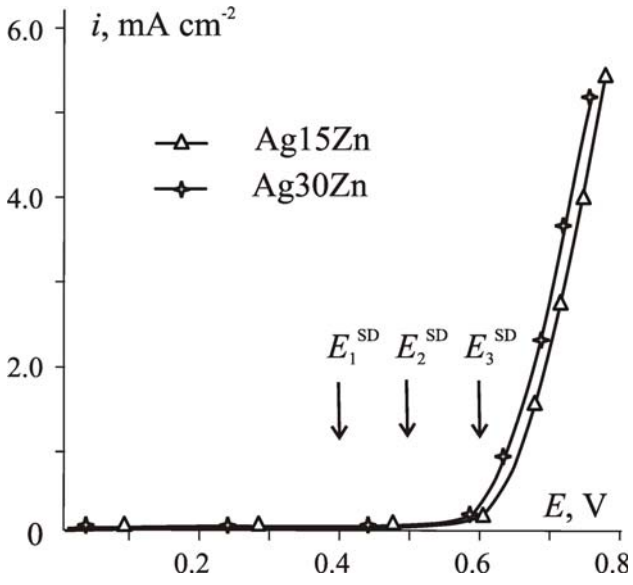

Fig. 1. Anodic voltammograms of Ag-Zn alloys in 0.01 M HNO_3 + 0.09 M KNO_3

$$L = \Psi M q_a/(zF\rho), \quad (2)$$

where M and ρ are the molar mass and density of the oxide; q_a is the density of the anodic charge; z is the number of electrons involved in oxide formation; F = 96485 C mol^{-1} is Faraday constant.

The control of surface morphology and composition was carried out using scanning electron microscope JSM 6380LV with micro-analysis system INCAx-sight 250 (JEOL, Japan)*. Images were obtained using the secondary electron mode with an accelerating voltage of 20 kV.

3. Results and Discussion

3.1. Anodic oxidation of Ag–Zn *alloys without preliminary selective dissolution*

On chronoamperograms obtained in deaerated 0.1 M KOH on silver and Ag–Zn alloys at a potential E = 0.56 V, a sharp and then smoother decrease of current was observed (Fig. 2a). At times greater than 10–20 s, the current density reached an almost constant value.

According to (2), for the formation of an Ag_2O film with an estimated thickness of 34 nm, assuming 100% current efficiency, it is necessary to accumulate a charge density of 20 mC cm^{-2}. Fig. 2a shows that with an increase in the initial concentration of zinc in the alloy, the polarization time required for the accumulation of a given charge density decreased.

With times not exceeding 5–10 s, linear sections in the coordinates, criterion for diffusion-limited processes were observed (Fig. 2b). A similar situation observed for pure silver and its alloys with gold allowed the authors of the study [19] to draw a conclusion about the solid-phase-diffusion control of the anode process. It should be assumed that on silver-zinc alloys, the anode process is controlled by mass transfer along the phase of the growing oxide as well.

In the general case, the recorded current and charge characterize not only the formation of Ag_2O oxide

$$2Ag + 2OH^- = Ag_2O + H_2O + 2\,e^-, \quad (3)$$

but also the transition of silver ions into the solution:

$$Ag + 2OH^- = Ag(OH)_2^- + e^-. \quad (4)$$

In addition, zinc oxidation, accompanied by the formation of an oxide or hydroxide film on the

* Centre for the Collective Use of Scientific Equipment of VSU.

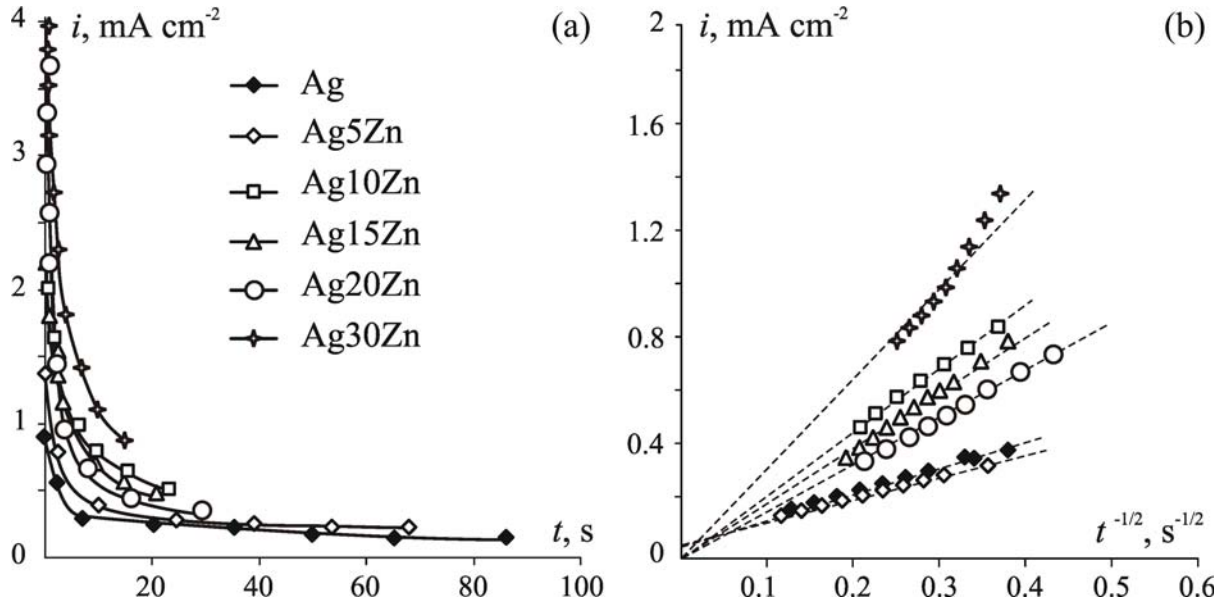

Fig. 2. Current transients of silver and Ag-Zn alloys in original (a) and Cottrell coordinates (b) in 0.1 M KOH at E_a = 0.56 V

surface of the electrode and ions in the electrolyte solution is possible:

$$Zn + 2OH^- = ZnO + H_2O + 2e^-; \quad (5)$$

$$Zn + 2OH^- = Zn(OH)_2 + 2e^-; \quad (6)$$

$$Zn + 4OH^- = Zn(OH)_4^{2-} + 2e^-. \quad (7)$$

In solutions with a high pH value (> 10), soluble products are formed:

$$ZnO + OH^- + H_2O = Zn(OH)_3^-; \quad (8)$$

$$ZnO + 2\ OH^- + H_2O = Zn\ (OH)_4^{2-}. \quad (9)$$

3.2. Measurement of open-circuit potential

Certain information regarding the nature and electrochemical behaviour of the oxide or hydroxide phase formed in 0.1 M KOH can be obtained using chronopotentiometry in open-circuit mode, carried out after the end of potentiostatic polarization (Fig. 3). When $N_{Zn} \leqslant 10$ at.% the open-circuit potential E_0 of oxidized alloys varies slightly over time and remains close to the values characteristic of Ag(I) oxide formed on silver. When concentration of zinc in the alloy increases, the potential E_0 shifts to less positive values. At the same time, a rather sharp decrease of potential over time was observed. Chemical dissolution of Ag(I) oxide can be the reason for a decrease in E_0:

$$Ag_2O + 2\ OH^- + H_2O = 2\ Ag\ (OH)_2^-. \quad (10)$$

The possibility of this process on silver and its alloys with gold was confirmed by the results of the photopotential measurement experiments [20–22].

3.3. Selective dissolution of Ag-Zn alloys

Chronoamperograms obtained on Ag15Zn and Ag30Zn alloys in 0.01 M HNO_3 + 0.09 M KNO_3 at various E^{SD} potentials had a similar shape. Typical current transients are shown in Fig. 4*a* for Ag15Zn alloy. During the anodic polarization, the current dropped to almost zero, reflecting the almost

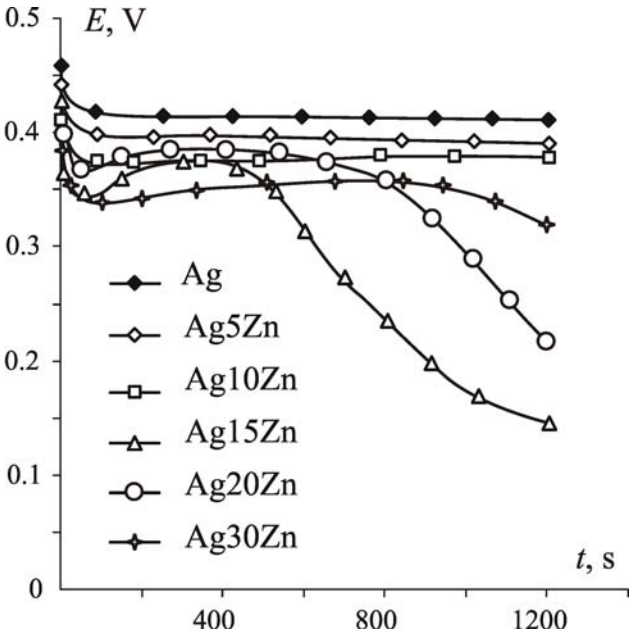

Fig. 3. Potential transients of silver and Ag-Zn alloys after the anodic oxidation in 0.1 M KOH

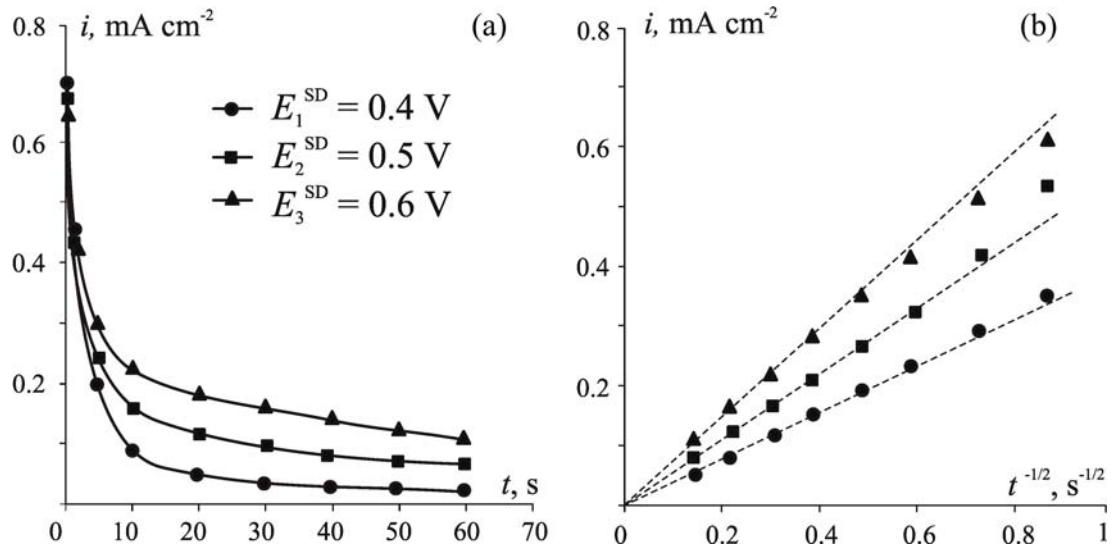

Fig. 4. Current transients of Ag15Zn in original (a) and Cottrell coordinates (b) at different E^{SD} in 0.01 M HNO_3 + 0.09 M KNO_3

complete dezincification of the surface layer of the alloy. The presence of linear sections in the Cottrell coordinates (Fig. 4*b*) allows applying SD chronoamperometry theory for the calculation of the diffusion coefficient and concentration of vacancies [15, 16]:

$$I(t) = \frac{z_A F N_A D_A^{1/2} S_g}{V_m \pi^{1/2} t^{1/2}} \left[1 - e^{-\frac{z_A F}{RT}\eta} \right]. \quad (11)$$

Here: I – current, t – time, z_A – the number of electrons involved in the oxidation of the electronegative component, N_A – volume concentration of atoms of component A in the alloy, $D_A = D_v N_v$ – diffusion coefficient of the atoms of component A in the surface layer of the alloy, D_v – diffusion coefficient of vacancies, N_v – concentration of vacancies, S_g – geometric surface area of the electrode, V_m – molar volume of the alloy, R = 8.314 J K^{-1} mol^{-1} – universal gas constant, T = 298 K – temperature, η – overvoltage.

The values of equilibrium vacancy concentrations equal to $2.55 \cdot 10^{-5}$ and $1.05 \cdot 10^{-5}$ at.% in Ag15Zn and Ag30Zn alloys, respectively, were obtained by thermodynamic calculations using data on the vacancy formation energy and their diffusion coefficients in individual metals [16].

Zinc diffusion coefficients D_A calculated according to (11) from the slopes $i,t^{-1/2}$-dependencies for each of the alloys increased with increase in E^{SD} (Table 2). According to the solid-phase-diffusion mechanism of SD, the reason for this is an increase in the concentration of superequilibrium vacancies (Table 2), e.g., the concentration of vacancy defects in the surface layer.

3.4. Anodic oxidation of Ag-Z**n** *alloys after selective dissolution*

Chronoamperograms obtained in 0.1 M KOH on alloys with different concentration of vacancy defects in the surface layer were similar in shape to chronoamperograms obtained on alloys without preliminary SD (not shown in the figures). Linear sections were also preserved in the criterion coordinates, indicating the transport nature of the limitations of the anode process in

Table 2. Diffusion coefficients of zinc D_A and concentration of superequilibrium vacancies N_v in the surface layer of Ag-Zn alloys at different potentials E^{SD}

Alloy	E^{SD}, V	D_A 10^{18}, cm^2 s^{-1}	N_v 10^4, at%
Ag15Zn	0.40	3.8	1.0
	0.50	8.1	2.1
	0.60	12.2	3.2
Ag30Zn	0.40	0.7	0.09
	0.50	1.1	0.1
	0.60	2.7	0.4

an alkaline environment. Most likely, the nature of the anodically formed products did not undergo significant changes during the transition from alloys without SD to alloys after SD.

3.5. The cathodic reduction of insoluble products of alloys oxidation

The cathodic voltammograms obtained on silver and alloys with an equilibrium concentration of vacancies after the end of anodic oxidation and change of solution in the cell are shown in Fig. 5a.

Considering the equilibrium potentials of processes (3)–(7), we can conclude that the maximum cathode current at potentials $E_{Ag(I)}$ = 0.32–0.36 V corresponds to the reduction process of Ag(I) oxide. A sharp increase in the cathode current associated with the onset of hydrogen emission was observed at potentials near –1.0 V, which was significantly higher than the equilibrium potentials of formation/reduction of zinc oxide or hydroxide (~ –1.3 V). Thus, if the products of zinc oxidation were also present in the oxide film on the alloys, then it was impossible to detect their presence using cathodic voltammograms.

When the cathodic reduction was preceded by a 20-minute stage of potential measurement in open-circuit mode, then the shape of voltammograms in general did not change (Fig. 5b). However, the peak of reduction of the Ag(I) oxide sharply decreased in amplitude, and it was absent on the Ag20Zn and Ag30Zn alloys. Indeed, on these alloys E_0 value was below $E_{Ag(I)}$ potentials of the reduction of Ag_2O. It should be assumed that the major volume of the formed oxide was already chemically dissolved according to (10) over the period of recording of the open-circuit potential.

If anodic oxidation was preceded by SD of alloys (stages 1′ and 2′), then E_0 and $E_{Ag(I)}$ potentials on cathodic voltammograms were shifted to more positive values characteristic for pure silver (Fig. 5c). The cathodic peak of reduction of the Ag(I) oxide was reliably fixed, and the absolute values of the maximum current were much higher than on alloys not subjected to preliminary SD.

5.6. The current efficiency of the anodic formation of Ag(I) *oxide*

The results of calculating the current efficiency according to (1) and the thickness of the Ag_2O films corrected to this value by (2) formed on silver and alloys of the Ag-Zn system after various stages of research are summarized in Tables 3 and 4. Cathodic charge Q_c characterizing the reduction of Ag(I) oxide was calculated according to the results of cathodic voltammetry (Fig. 5a, b, c) in the potential region from E_0 up to E = 0.20 V.

The current efficiency of anodic oxide formation on alloys without SD (Table 3) was lower than on silver, and decreased with increasing zinc concentration in the alloy. Accordingly, the thickness of the Ag(I) oxide also decreased from 32 to 5.8 nm during the transition from Ag to Ag30Zn. The decrease in current efficiency with increasing zinc concentration can be explained by an increase in the porosity of the oxide film. As a result, the possibility of dissolution of silver through the pores increased, the fraction of the current used for the formation of silver ions entering the solution

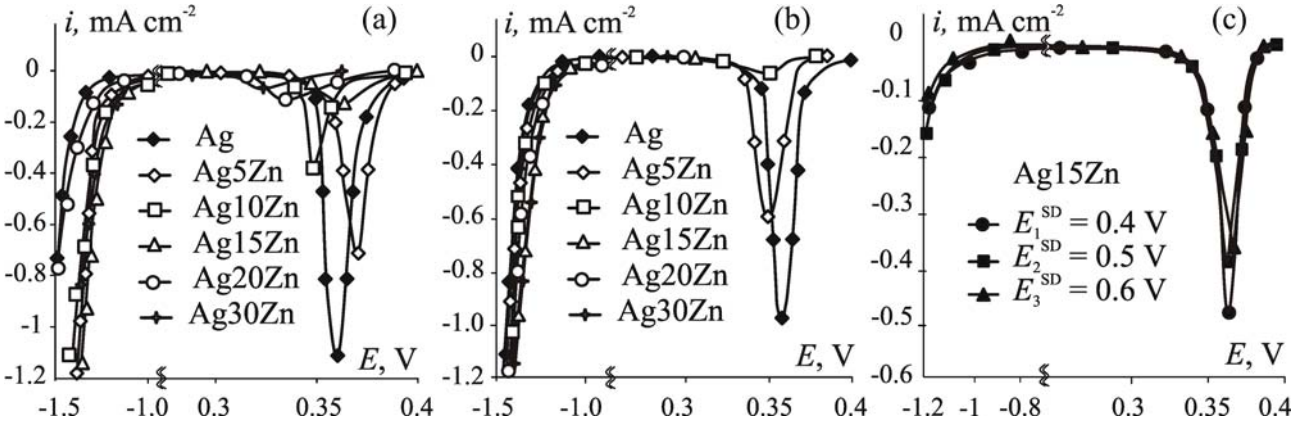

Fig. 5. Cathodic voltammograms of silver and Ag-Zn alloys after the anodic polarization at E_a = 0.56 V and change of the solution: (a) without an open-circuit stage; (b) after the open-circuit stage and after the preliminary selective dissolution of Ag15Zn (c)

Table 3. Current efficiency Ψ and thickness L of Ag(I) oxide, anodically formed on silver and alloys without preliminary SD

N_{Zn}, at. %	Without an open-circuit stage		After the open-circuit stage	
	Ψ, %	L, nm	Ψ*, %	L^*, nm
0	94.4	32.0	89.1	30.3
5	70.7	24.0	65.5	22.3
10	39.4	13.0	28.7	9.6
15	28.0	9.5	28.2	9.6
20	24.6	8.4	8.1	2.8
30	16.2	5.8	5.4	1.8

Table 4. Current efficiency Ψ^{SD} and thickness L^{SD} of Ag(I) oxide, anodically formed on Ag15Zn and Ag30Zn after the preliminary SD

N_{Zn}, at. %	E^{SD}, V	Ψ^{SD}, %	L^{SD}, nm
15	0.4	53.2	18.1
	0.5	47.9	16.3
	0.6	43.3	14.7
30	0.4	12.4	4.2
	0.5	8.1	2.8
	0.6	3.5	1.7

increased, and the fraction of the current used for the formation of the film decreased.

After a 20 min exposure in open circuit mode, the current efficiency values of Ψ* calculated from (1) and oxide thickness L^* determined by (2) further decreased (Table 3), which confirms the assumption of the chemical dissolution of silver oxide in an alkaline medium.

The current efficiency of anodic oxide formation on alloys subjected to preliminary SD (Table 4) was lower than that on silver, but higher than that on alloys without preliminary SD. As the potential of SD increased, i.e., increased concentration of vacancy defects in the surface layer of the alloy, the current efficiency and thickness of the Ag(I) oxide decreased.

3.7. Morphology of anodically formed films

Comparison of the results of energy-dispersive microanalysis conducted on the alloys before the start of their anodic oxidation and after its completion demonstrated an increase in the oxygen concentration in the surface layer (Table 5), which confirms the presence of an oxide layer on the surface.

The thickness of the oxide intended for SEM was increased to 120 nm, taking into account the obtained current efficiency values. Typical SEM images of the oxidized surface for Ag15Zn and Ag30Zn without SD (Fig. 6a, b) and for the same alloys, but subjected to preliminary SD at the potential E_2^{SD} (Fig. 6 c, d) are presented. On the surface of all alloys, individual particles of the oxide phase can be observed; the particle shape was close to spherical. Depending on the initial concentration of zinc in the alloy and the conditions for preparing the surface for oxidation, the particles size and quantity on the unit of the electrode surface changed.

On alloys not subjected to preliminary SD, a decrease in the particle diameter of the formed

Table 5. The composition (at.%) of the alloy samples before and after the anodic oxidation

Stage	Element	Alloy				
		Ag5Zn	Ag10Zn	Ag15Zn	Ag20Zn	Ag30Zn
Before oxidation	Ag	93.77	89.32	85.99	77.84	71.36
	Zn	6.23	10.68	14.01	22.16	28.64
After oxidation	Ag	54.23	61.66	52.45	38.50	40.27
	Zn	2.90	8.30	7.81	11.23	15.86
	O	42.87	30.03	39.74	50.27	43.87

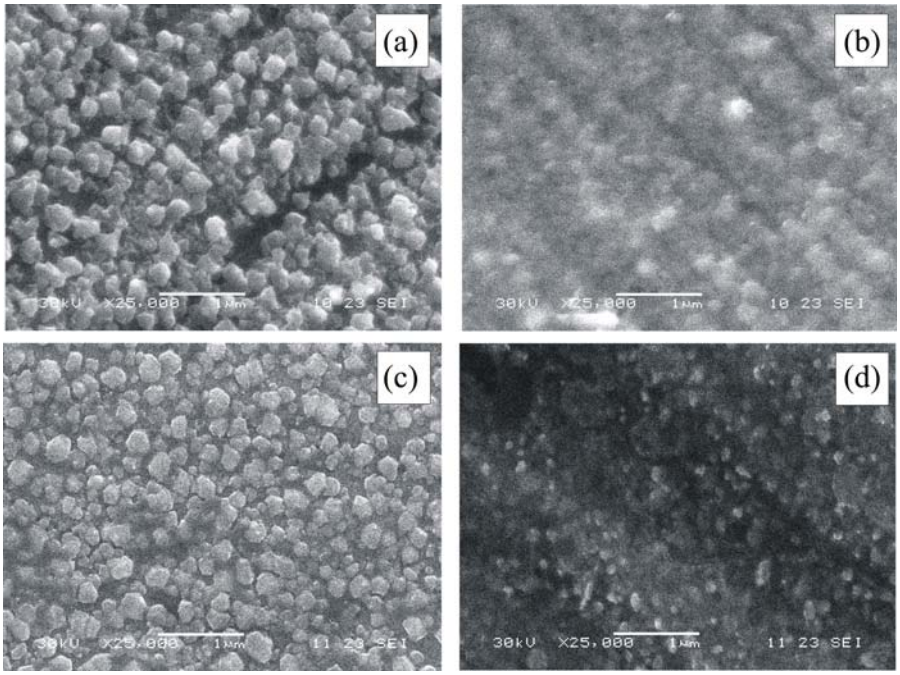

Fig. 6. SEM images of Ag(I) oxide, anodically formed on Ag15Zn (a), (c) and Ag30Zn (b), (d) in 0.1 M KOH at E_a = 0.56 V without SD (a), (b) and after preliminary SD at E_2^{SD} = 0.50 V (c), (d)

oxide with increasing zinc concentration was revealed (Table 6). Probably this situation was associated with a decrease in the interatomic distance of Ag-Ag from 0.409 to 0.403 nm with increasing N_{Zn} from 0 to 30 at.% [23]. At the same time, an increase in the oxide particles quantity on the unit of the electrode surface was observed.

Upon transition to alloys subjected to preliminary SD, the particles diameter decreased, and the particles quantity on the unit of the electrode surface increased (Table 6). In this case, a decrease in the particle size of the Ag(I) oxide probably was associated with an increase in the concentration of vacancy defects in the surface layer of alloys. It is not possible to trace a clear trend of decreasing oxide particles diameter or increasing their quantity on the unit of the electrode surface with increasing zinc concentration on alloys after SD.

4. Conclusions

1. Ag(I) oxide is the main product of the anodic dissolution in an aqueous alkaline medium of homogeneous polycrystalline alloys of the Ag-Zn system (α-phase), as well as these alloys, but subjected to preliminary selective dissolution of zinc from their surface layer in an acidic medium.

2. Silver-zinc alloys with enriched to almost pure silver, but with a structurally-disordered surface layer, are characterized by increased current efficiency of the anodic oxide formation process, as well as a higher thickness of Ag(I)

Table 6. Diameter d of Ag_2O particles and their quantity P on the unit of the electrode surface

Stage	Parameter	Electrode					
		Ag	Ag5Zn	Ag10Zn	Ag15Zn	Ag20Zn	Ag30Zn
Without SD	d, nm	350	200	170	180	200	170
	P, μm^{-2}	13	13	13	21	28	21
E_1^{SD}	d, nm	–	95	100	90	90	100
	P, μm^{-2}	–	111	44	101	68	79
E_2^{SD}	d, nm	–	160	110	110	120	100
	P, μm^{-2}	–	44	59	59	87	70
E_3^{SD}	d, nm	–	90	100	95	90	95
	P, μm^{-2}	–	70	70	71	67	60

oxide in comparison with equilibrium alloys of the same chemical composition. At the same time, these characteristics turn out to be noticeably lower in comparison with compact polycrystalline silver.

3. Ag(I) oxide, anodically formed on silver and silver-zinc alloys (α-phase) of not only the initial composition, but also after the selective dissolution of zinc from their surface layer, is chemically unstable in an alkaline medium.

4. The diameter of the anodically formed Ag(I) oxide particles decreases, and their quantity on the unit of the electrode surface increases with an increase in the concentration of vacancy defects in the surface layer of the alloy.

Acknowledgments

The results of the research were obtained using the Centre for the Collective Use of Scientific Equipment of Voronezh State University. URL: http://ckp.vsu.ru

Conflict of interests

The authors declare that they have no known competing financial interests or personal relationships that could have appeared to influence the work reported in this paper.

References

1. Gao X.-Y., Wang S.-Y., Li J., Zheng Y.-X., Zhang R.-J., Zhou P., Yang Y.-M., Chen L.-Y. Study of structure and optical properties of silver oxide films by ellipsometry, XRD and XPS methods. *Thin Solid Films*. 2004;455-456: 438-442. DOI: https://doi.org/10.1016/j.tsf.2003.11.242

2. Mehdi H. E., Hantehzadeh M. R., Valedbagi Sh. Physical properties of silver oxide thin film prepared by DC magnetron sputtering: effect of oxygen partial pressure during growth. *J. Fusion Energy*. 2013;32(1): 28–33. DOI: https://doi.org/10.1007/s10894-012-9509-5

3. Ferretti A. M., Ponti A., Molteni G. Silver(I) oxide nanoparticles as a catalyst in the azide–alkyne cycloaddition. *Tetrahedron Letters*. 2015;56(42): 5727-5730. DOI: https://doi.org/10.1016/j.tetlet.2015.08.083

4. Klingshirn C. F., Meyer B. K., Waag A., Hoffmann A., Geurts J. *Zinc oxide. From fundamental properties towards novel applications*. Berlin: Springer; 2010. 374 p.

5. Wei J., Lei Y., Jia H., Cheng J., Hou H., Zheng Z. Controlled in situ fabrication of Ag_2O/AgO thin films by a dry chemical route at room temperature for hybrid solar cells. *Dalton Trans*. 2014;43(29): 11333–11338. DOI: https://doi.org/10.1039/C4DT00827H

6. Shuaishuai M., Jinjuan X., Yuming Z., Zewu Z. Photochemical synthesis of ZnO/Ag_2O heterostructures with enhanced ultraviolet and visible photocatalytic activity. *J. Mater. Chem. A*. 2014;2(20): 7272–7280. DOI: https://doi.org/10.1039/C4TA00464G

7. Shahriary L., Athawale A. A. Electrochemical deposition of silver/silver oxide on reduced graphene oxide for glucose sensing. *J. Solid State Electrochem*. 2015;19(8): 2255–2263. DOI: https://doi.org/10.1007/s10008-015-2865-0

8. Istomina O. V., Evstropiev S. K., Kolobkova E. V., Trofimov A. O. Photolysis of diazo dye in solutions and films containing zinc and silver oxides. *Optics and Spectroscopy*. 2018;124(6): 774–778. DOI: https://doi.org/10.1134/S0030400X18060097

9. Xiang Q., Meng G., Zhang Y., Xu J., Xu P., Pan Q., Yu W. Ag nanoparticle embedded-ZnO nanorods synthesized via a photochemical method and its gas-sensing properties. *Sens. Actuators B*. 2010 ;143(2): 635–640. DOI: https://doi.org/10.1016/j.snb.2009.10.007

10. Meng F., Hou N., Jin Z., Sun B., Guo Z., Kong L., Xiao X., Wu H., Li M., Liu J. Ag-decorated ultra-thin porous single-crystalline ZnO nanosheets prepared by sunlight induced solvent reduction and their highly sensitive detection of ethanol. *Sens. Actuators B*. 2015;209: 975–982. DOI: https://doi.org/10.1016/j.snb.2014.12.078

11. Kaesche H. *Corrosion of metals*. Berlin: Springer-Verlag; 2012. 594 p.

12. McCafferty E. *Introduction to corrosion science*. New York: Springer; 2010. 583 p.

13. Marcus P. *Corrosion mechanisms in theory and practice*. New York: Marcel Dekker; 2002. 729 p.

14. Marshakov I. K., *Termodinamika i korroziya splavov* [Thermodynamics and corrosion of alloys]. Voronezh: VSU Publishing House; 1983. 166 p. (In Russ.)

15. Marshakov I. K., Vvedensky A.V., Kondrashin V. Yu., Bokov G. A. *Anodnoe rastvorenie i selektivnaya korroziya splavov* [Anodic dissolution and selective corrosion of alloys]. Voronezh: VSU Publishing House; 1988. 402 p. (In Russ.)

16. Kozaderov O. A., Vvedensky A. V. *Massoperenos i fazoobrazovanie pri anodnom selektivnom rastvorenii gomogennykh splavov* [Mass transfer and phase formation during anodic selective dissolution of homogeneous alloys]. Voronezh: Nauchnaya kniga; 2004. 288 p. (In Russ.)

17. Vvedenskii A. V., Kozaderov O. A. Linear voltammetry of anodic selective dissolution of homogeneous metallic alloys. In: Saito Y., Kikuchi T. (eds.) *Voltammetry: theory, types and applications*. New York: Nova Science Publishers, Inc.; 2014. 363 p.

18. Murtazin M. M., Nesterova M. Yu., Grushevskaya S. N., Vvedensky A. V. Silver(I) oxide on silver-zinc alloys: anodic formation and properties. *Electrochemistry*. 2019;55(7): 873–884. DOI: https://doi.org/10.1134/S0424857019070089 (In Russ.)

19. Vvedenskii A., Grushevskaya S., Kudryashov D., Kuznetsova T. Kinetic peculiarities of anodic dissolution of silver and Ag-Au alloys under the conditions of oxide formation. *Corrosion Science*. 2007;49: 4523–4541. DOI: https://doi.org/10.1016/j.corsci.2007.03.046

20. Kudryashov D. A., Grushevskaya S. N., Vvedensky A. V. *Fotopolyarizatsiya v anodnom okside Ag2O na serebre pri UF-obluchenii* [Photopolarization in anodic oxide Ag_2O on silver under UV irradiation]. *Kondensirovannye sredy i mezhfaznye granitsy = Condensed Matter and Interphases*. 2005;7(2): 141–149. Available at: http://www.kcmf.vsu.ru/resources/t_07_2_2005_006.pdf (In Russ.)

21. Kudryashov D. A., Grushevskaya, S. N., Vvedenskii A. V. Determining some structure-sensitive characteristics of nano-sized anodic Ag(I) oxide from photopotential spectroscopy. *Protection of Metals*. 2007;43: 591–599. DOI: https://doi.org/10.1134/S0033173207060124

22. Kudryashov D. A., Grushevskaya S. N., Olalekan O., Kukhareva N. V., Vvedenskii A. V. Effect of orientation of crystal face of silver and its alloying with gold on properties of thin anodic Ag(I) oxide films: II. Photopotential. *Protection of Metals and Physical Chemistry of Surfaces*. 2010;46(1): 32–39. DOI: https://doi.org/10.1134/S2070205110010041

23. Pearson W. B. *A Handbook of lattice spacing sand structures of metals and alloys*. London: Pergamon Press; 1958. 1044 p.

Information about the authors

Svetlana N. Grushevskaya – PhD in Chemistry, Associate Professor, Department of Physical Chemistry, Voronezh State University, Voronezh, Russian Federation; e-mail: sg@chem.vsu.ru. ORCID iD: https://orcid.org/0000-0002-7083-1438.

Aleksander V. Vvedenskii, DSc in Chemistry, Professor, Department of Physical Chemistry, Voronezh State University, Voronezh, Russian Federation; e-mail: alvved@chem.vsu.ru. ORCID iD: https://orcid.org/0000-0003-2210-5543.

Valeria O. Zaitseva, 5th year student of the Faculty of Chemistry, Voronezh State University, Voronezh, Russian Federation; e-mail: valera.zaytseva.00@mail.ru.

All authors have read and approved the final manuscript.

Translated by Valentina Mittova.
Edited and proofread by Simon Cox.